Monolithic Integrated Semiconductor Optical Amplifier With Broad Spectrum, High Power, and Small Linewidth Expansion

XIN LI[1,2], LEI LIANG[1,2], LI JUN WANG[1,3,4], LI QIN[1,2], YONG YI CHEN[1,2], YU BING WANG[1,2], YUE SONG[1,2], YU XIN LEI[1,2], PENG JIA[1,2], YU GANG ZENG[1,2], CHUAN TAO ZHENG[5], AND HUAN ZHAO[5]

[1]State Key Laboratory of Luminescence and Applications, Changchun Institute of Optics, Fine Mechanics and Physics, Chinese Academy of Sciences, Changchun 130033, China
[2]Center of Materials Science and Optoelectronics Engineering, University of Chinese Academy of Sciences, Beijing 100049, China
[3]Peng Cheng Laboratory, Shenzhen 518000, China
[4]Key Laboratory of Laser Technology and Optoelectronic Functional Materials of Hainan Province, Academician Team Innovation Center of Hainan Province, School of Physics and Electronic Engineering, Hainan Normal University, Haikou, Hainan 570206, China
[5]State Key Laboratory on Integrated Optoelectronics, College of Electronic Science and Engineering, Jilin University, Changchun 130012, China

Corresponding author: Lei Liang (liangl@ciomp.ac.cn)

ABSTRACT Semiconductor optical amplifiers (SOAs) offer direct electrical injection, power consumption, integration, and anti-radiation advantages over optical fiber amplifiers. However, saturation output power and gain bandwidth have been limited in traditional structure SOAs. We demonstrate a monolithic integrated SOA with broad spectrum, high power, high gain, and small spectral linewidth expansion. The device adopts a two-stage amplified large optical cavity structure, and a lower optical field confinement factor is obtained by adjusting the thickness of the waveguide layer. The lower optical field confinement factor is conducive to improving the coupling efficiency and the maximum output power. Our device, fabricated only by standard i-line lithography with micron-scale precision, obtains excellent and stable performance. When the input power is set to 1 mW, the output power is 419 mW with a gain of 26.23 dB. When the input power is set to 25 mW at 25 °C, the output power increases to 600 mW with a gain of 13.8 dB. The corresponding gain bandwidth of 3 dB measures at least 70 nm. The spectral linewidth after the SOA is 1.15 times wider than that of the seed laser.

INDEX TERMS Broad spectrum, high gain, high power, semiconductor optical amplifiers, small linewidth expansion.

I. INTRODUCTION

High-power optical amplifiers are required for an increasing number of applications, including free space optical communication, light laser detection and ranging (lidar), absorption spectroscopy, biomedical imaging, microwave photonic (MWP) analog signal processing, and low-noise mode-locked lasers for photonic analog-to-digital

The associate editor coordinating the review of this manuscript and approving it for publication was San-Liang Lee.

converters [1]–[8]. These applications most commonly utilize solid-state or doped-fiber as the gain medium [9], [10]; 50 W and greater than 150 W erbium-doped fiber amplifiers (EDFAs) have been demonstrated in the 1550 nm wavelength optical communications commercial field. In addition to high power, EDFAs also exhibit superior noise performance due to their large intracavity powers, small intracavity losses, and negligible gain/index coupling [11]–[13]. However, the main material of the fiber amplifier is silica, which has poor radiation hardness. Currently, the common

materials require reinforced packaging to reduce radiation, which increases the volume and weight, and is disadvantageous for integration. In addition, the fiber amplifier power conversion efficiency due to optical pumping is low, which greatly limits the wider and more advanced applications of fiber optic amplifiers.
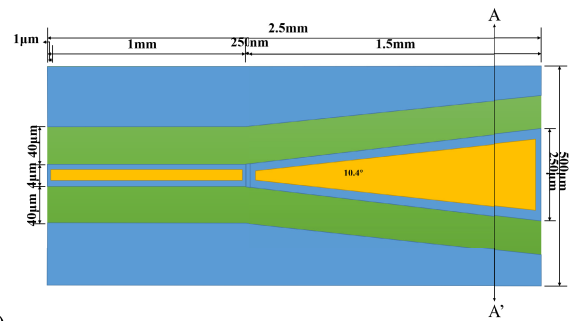
Compared with optical fiber amplifiers, semiconductor optical amplifiers (SOAs) have many advantages, including greater compactness, smaller volume and weight, higher power conversion efficiency, larger gain bandwidth, wavelength designability, and the potential for monolithic integration of SOAs with other components (e.g., lasers, modulators, and detectors) [14]–[21]. More importantly, the radiation hardness of Group III and V materials is 6 to 7 times higher than that of silica, making them more suitable for space applications. In the fields of on-chip all-solid-state lidar and space laser communication for long-rang sensing [22], SOAs with 0.5 W or higher output power and larger and flatter gain spectrum range are more suitable and promising.

In this paper, a two-stage monolithic integrated SOA with high saturation output power, wide gain bandwidth, and low noise figure is proposed. The design of the device is described in Section 2, including the epitaxial structure design, waveguide design, electrothermal analysis, and gain characteristics analysis. The experimental setup and device performance are characterized in Section 3, and the performance is compared with that of similar devices in Section 4. Finally, the conclusion is presented in Section 5.
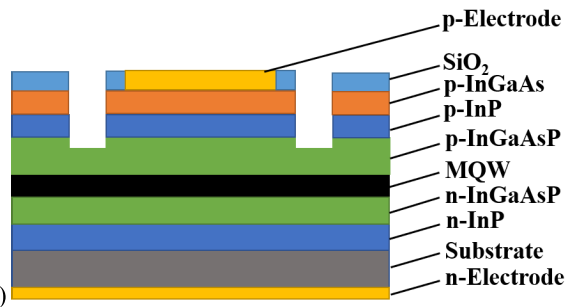
II. STRUCTURAL DESIGN

Fig. 1 shows the schematic diagram of the proposed broad-spectrum, high-power, high-gain, small linewidth expansion SOA epitaxial structure. The epitaxial structure of the SOA uses InAlGaAs material in the active region, and the waveguide layer adopts a graded waveguide that can improve the carrier injection efficiency while further increasing the limit of carriers in the active region. The composition gradient is applied in the heterojunction interface of the epitaxial layer to reduce the barrier height of the heterojunction interface and the series resistance of the SOA.

To provide more carriers to prevent gain saturation, a two-stage SOA with a 2.5 mm cavity length and 1 mm width was designed as shown in Fig. 1(a) to include two waveguides: a 1 mm long and 4 μm wide ridge waveguide and a 1.5 mm long tapered waveguide with an inclination angle of 10.4°. The width of the tapered output facet is 250 μm and each waveguide is connected to electricity separately. The isolation trench width is 40 μm. The distance between the electrode and the mesa is 1 μm, and the distance between the ridge waveguide and the tapered waveguide is 250 nm. As the light propagates from the input facet of the amplifier to the output facet, the width of the waveguide gradually increases; this structure ensures that most of the light remains in the default mode and provides gain with a high saturation output power while reducing heat generation and catastrophic optical damage (COD). To suppress the deterioration of the cavity
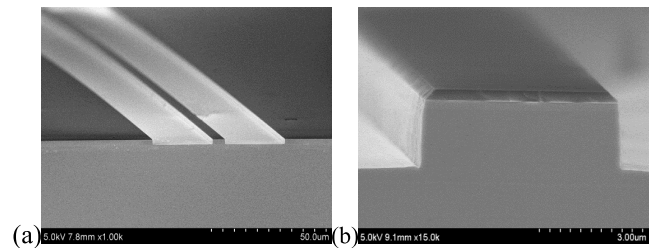

(a)

(b)

FIGURE 1. (a) SOA device top view. (b) The cross-section diagram of SOA at AA' in Fig. 1(a).

FIGURE 2. Scanning electron microscope images of the mesa of the ridge waveguide (a) etched at a 45° angle and (b) magnified topography.

facets and increase the output power, the two cavity facets of the SOA are coated with an optical anti-reflective coating (reflectance of 0.01%). The coating on the cavity facets also reduces COD. The shape of the ridge waveguide etched mesa can be observed by scanning electron microscopy. Fig. 2(a) shows the mesa etched at a 45° angle, and Fig. 2(b) shows the topography of the etched mesa. The ridge waveguide has a regular and flat morphology, and the sidewall has a slope of 85° or more.

The optical field confinement factor in the active area is the ratio of the overlap between the optical field and the active area to the overall optical field distribution [23]. Fig. 3 shows distribution of the optical field and refractive index of the two active area optical field confinement factor structures. The optical field confinement factor in Fig. 3(a) is larger than in Fig. 3(b). Structures with larger optical field confinement factors will confine more photons to the active area, and structures with smaller optical field confinement factors will allow more photons to leak into the waveguide layer. In this paper, the structure displayed in Fig. 3(b) was adopted, with the
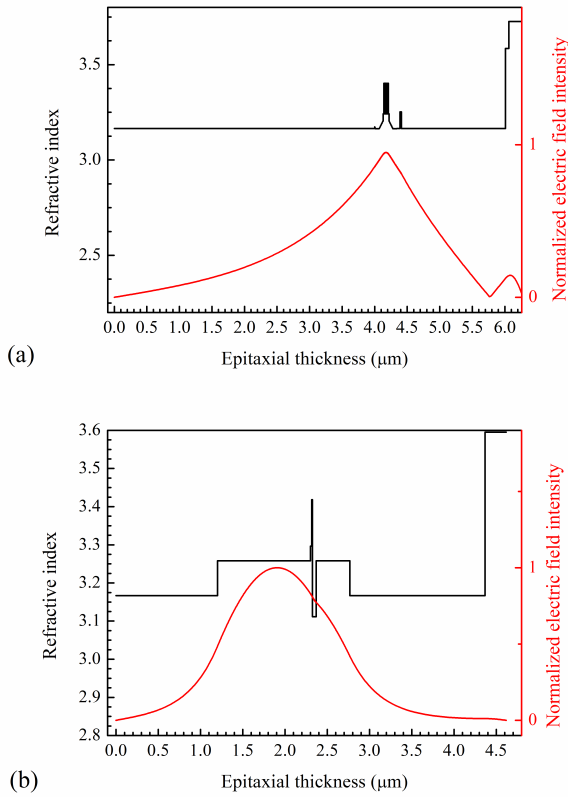
FIGURE 3. Distribution of the optical field and refractive index. Optical field confinement factor of the active area: (a) Γ = 2.43%; (b) Γ = 0.47%.

FIGURE 4. Distribution of the optical field. Optical field confinement factor of the active area: (a) Γ = 2.43%; (b) Γ = 0.47%.

refractive index of the waveguide layer and the cladding layer at 3.258 and 3.167 respectively. By increasing the thickness of the waveguide structure, the optical field distribution over the entire epitaxial region is enlarged to reduce the optical field confinement factor and the far-field vertical divergence angle. In addition, the thicker the waveguide, the less overlap between the optical field and the heavily doped confinement area, which reduces light loss, increasing electro-optic conversion efficiency to some extent and generating less heat.

To analyze the effect of waveguide structure on the optical field distribution, the effective refractive index method was applied using COMSOL Multiphysics for further simulation of the confinement factor of the optical field in the active area. There is a clear difference in the optical field distribution when the confinement factors are different in the same waveguide structure, as shown in Fig. 4. Fig. 4(a) shows the optical field distribution with the confinement factor Γ = 2.43% in the active region. A small spot size and the location of the highest luminous intensity within the active region are observed. Fig. 4(b) displays the optical field distribution in the active region with the confinement factor Γ = 0.47%. Due to the reduction in the optical confinement factor, the upper and lower waveguide layers and active region form a weak waveguide structure. It is observed that when the size of the optical field distribution is large, the optical field intensity expands to the upper and lower waveguide layers, and the location where the optical field intensity is
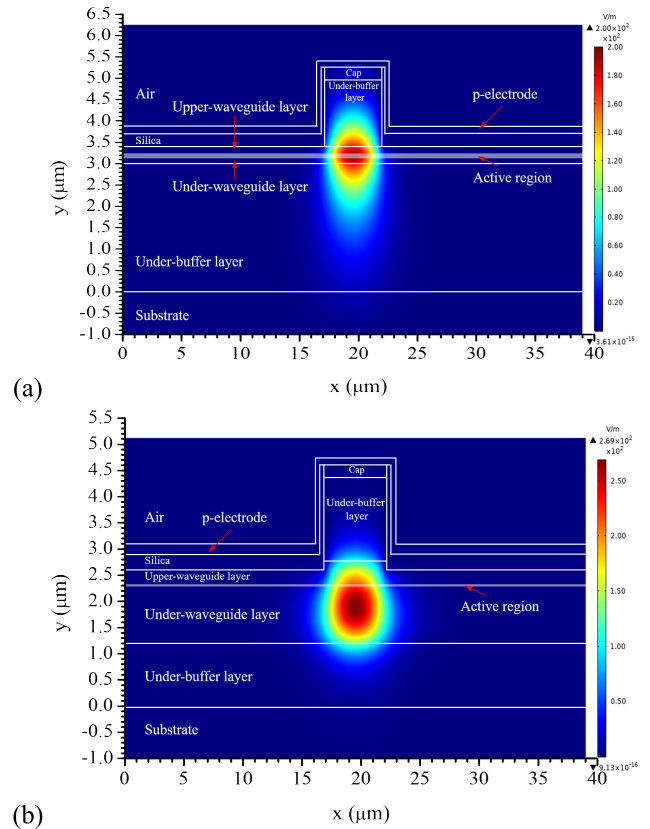
highest deviates from the active area and reaches the lower waveguide layer. In summary, the low confinement factor is useful for obtaining the mode field distribution matched with single-mode fiber and increasing the maximum output power. Therefore, the SOA studied in this paper adopts the active region structure with a confinement factor Γ = 0.47% as shown in Fig. 4(b).

There is a waveguide effect in a plane perpendicular to the P–N junction due to the refractive index step change Δn_R at the heterojunction interface. The waveguide effect is related to the temperature distribution ΔT and the free carrier concentration ΔN_{fc}. When the SOA starts working, the temperature and free carrier concentration change to satisfy the following relationship:

$$\Delta n_R = \alpha_T \cdot \Delta T - \alpha_{fc} \cdot \Delta N_{fc} \qquad (1)$$

where α_T is the temperature correlation coefficient and α_{fc} is the free carrier concentration correlation coefficient. The free carrier concentration prevails when the SOA begins operation, and Δn_R is a negative value; when the SOA operates longer, the temperature distribution predominates, and Δn_R is a positive value. The relationship between the etch depth and the single-mode width of the device for several values of the refractive index difference at the active region is shown in Fig. 5. The area under the curve represents the single-mode area with the refractive index change. In this paper, the etch
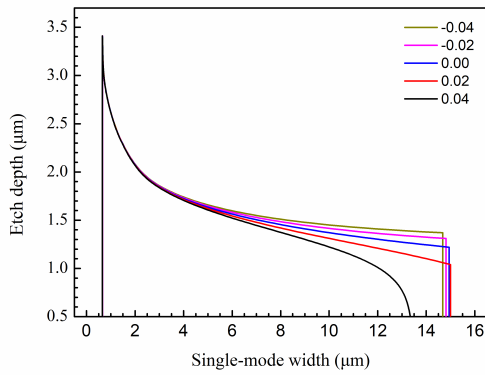
FIGURE 5. Relationship between the etch depth of the device and the single-mode width for various values of the refractive index change at the heterojunction interface.

depth of the SOA is 1.5 μm, and the single-mode width is 5 μm.

As the performance of SOAs continues to improve, the effect of internal thermal effects on device performance becomes more evident, and this has become one of the key factors limiting the operating characteristics of SOAs. When continuous current is applied to the SOA, the temperature of the active area rises due to severe internal heat build-up, resulting in a red shift in the wavelength, an increase in the threshold current, a decrease in output power, and a shortened device lifetime. Therefore, thermal analysis of the device is essential.

The heat generated in the active area inside the SOA is mainly generated in four parts, which can be expressed as

$$Q_{active} = Q_{thermal} + Q_{leak} + Q_{rec} + Q_{abs} \quad (2)$$

After the current is injected into the active region, the barrier layer has a higher energy band position than the quantum well layer, so these carriers are injected into the active region, and the carriers injected into the quantum well at the barrier create an energy difference. The energy difference is dissipated in the form of heat. This part of the heat source density can be expressed as

$$Q_{thermal} = [(E_B - E_L)\eta_i]j_b/q \quad (3)$$

where E_L is the forbidden band width of the quantum well, E_B is the forbidden band width of the barrier layer, j_b is the injection current density, η_i is the internal quantum efficiency of the active region, and q is the electronic charge.

Because the injected carriers cannot be completely captured by the quantum well, some electrons or holes leak to the outside of the quantum well. These leaked carriers will recombine with the holes or electrons in the barrier region to generate photons that have a large energy and are easily absorbed to produce heat. This part of the thermal power density can be expressed as

$$Q_{leak} = E_B(1 - \eta_i)j_b/q \quad (4)$$

Additionally, some of the carrier electrons or holes injected into the quantum well are not fully utilized; this part of the

energy is also part of the heat source, and the expression for the heat generation of this part is

$$Q_{rec} = E_L\eta_i j_{th}/q \quad (5)$$

where j_{th} is the threshold current density. In addition, when the SOA works normally, the laser generating area will cause strong light absorption, which is mainly concentrated in the active area, and this part of the heat generation can also be included in the total active area heat generation.

$$Q_{abs} = \frac{\eta_i(j_b - j_{th})\alpha_i E_L}{q(\alpha_i + \alpha_m)} \quad (6)$$

where α_i and α_m represent the internal loss and cavity facets loss of the SOA, respectively. By analyzing the various heat generation mechanisms caused by the SOA carrier injection, the epitaxial structure of the SOA device can be further optimized to achieve better performance. The waveguide layer adopts a graded waveguide, which can improve the carrier injection efficiency while further improving the limitation of carriers in the active region. The composition gradient is adopted at the heterojunction interface of the epitaxial layer to reduce the barrier height of the interface, reducing series resistance and heat. Coating the two cavity facets of the amplifier with optical anti-reflection coating reduces the cavity facet loss, thereby reducing heat generation, and also reducing the COD.

Gain is an important index of SOA performance. Typically, both the cavity facets of the SOA are used in an ideal anti-reflection method, allowing the incident light signal to receive only single-pass amplification. The single-pass gain obtained by the external optical signal in the SOA is expressed as

$$G_s = \exp[(\Gamma g - \alpha_i)L] \quad (7)$$

where L is the length of the SOA active region, and g and α_i are the gain and loss factors. However, the SOA has a constant residual reflectance at both facets, can form a Fabry–Pérot cavity on its own, and has a constant resonance effect, and it is also difficult to obtain a full single-pass amplification of the external optical signal. The gain of the SOA with the facet reflectances R_1 and R_2 is expressed as a function of the single-pass gain G_s as

$$G = \frac{(1 - R1)(1 - R2)G_s}{(1 - G_s\sqrt{R1R2}) + 4\sqrt{R1R2}G_s \sin^2 \phi} \quad (8)$$

where ϕ is the change of output phase shift. Anti-reflective coatings are usually used on both facets, but there is still some residual reflectance, causing ripples to appear in the gain spectrum. The peak-to-valley ratio between the resonant gains is called the SOA gain variation G_r, which is expressed as

$$G_r = \frac{1 + G_s\sqrt{R1R2}}{1 - G_s\sqrt{R1R2}} \quad (9)$$

For an ideal SOA, both R_1 and R_2 are 0 and G_r is 1. This means that there is no fluctuation in the resonant cavity mode frequency. But the real situation is not ideal.
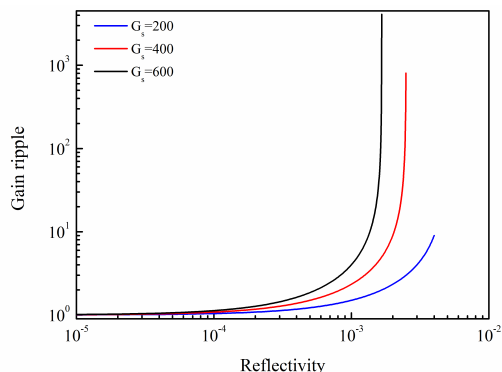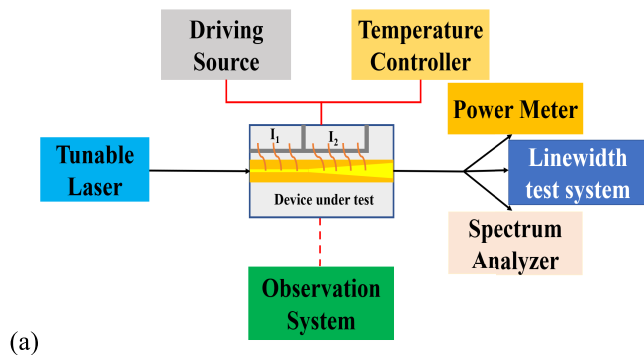
FIGURE 6. Relationship between gain variation and reflectance for three single-pass gains (G_s =200, 400, and 600).

Fig. 6 shows the relationship between gain variation and reflectance. As the gain increases or the cross-sectional reflectance increases, the gain fluctuation increases. Therefore, reducing the reflectance of the two cavity facets reduces the effect of gain fluctuations. The two cavity facets of the SOA in this paper are coated with an optical anti-reflective coating (reflectance of 0.01%).
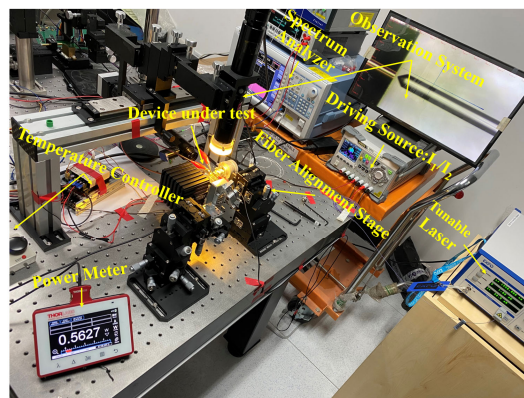
III. DEVICE PERFORMANCE TESTING AND ANALYSIS

The device in this study was grown by metal-organic chemical vapor deposition (MOCVD) and was fabricated using only ordinary i-line lithography to simplify the difficulty of fabrication without using complex fabrication steps such as expensive and time-consuming epitaxy regrowth fabrication technology. Moreover, excellent performance and stable operation were still achieved with the simple and low-cost technology. Fig. 7(a) illustrates the experimental setup for performance testing of the proposed two-stage monolithic integrated SOA at 25 °C. The device used Ti/Pt/Au as the p-side electrode and Au/Ge/Ni/Au as the n-side electrode, and the device was welded to the heat sink with the n-side facing down to form an ohmic contact, which was mounted to a thermoelectric cooling (TEC)-controlled stage. The tunable laser output was connected to the SOA through a fiber, and a spectrum analyzer was used to obtain the spectrum of the light amplified by the SOA through a fiber. For optical power measurements, the fiber was removed from the front of the SOA and replaced with a power meter. The ridge waveguide and tapered waveguide had separate electrical contacts. The currents into the ridge waveguide (I_1) and tapered waveguide (I_2) of the SOA were continuous. Fig. 7(b) displays a photograph of the experimental setup.

Maintaining a single mode is essential for both lasers and SOAs. The main function of the ridge waveguide is to maintain the single mode, and the current I_1 connected to the ridge waveguide was fixed in this study because it was confirmed that the current change in the ridge waveguide had little effect on the performance of the device [23]. The magnitude of the current I_2 connected to the waveguide region was used to test the performance of the device.

(a)

(b)

FIGURE 7. Experimental setup for testing the SOA. (a) Schematic diagram. (b) Photograph of the experimental setup.

The previous analysis shows that ideally the effective facet reflectivity of the SOA should be zero, so that the photons will not generate resonance amplification in the gain medium. However, it is impossible to achieve in practice, and even a small reflection will cause some disturbance in the amplified spontaneous emission (ASE) spectrum. The ASE of the SOA is characterized by using an optical spectrum analyzer (OSA). The bias current I_1 was 0.3 A, and I_2 was set to 1.5 A, 2.0 A, and 2.5 A to obtain the ASE spectra shown in Fig. 8. When the attenuation rate of the upper-level particles due to amplified spontaneous emission is similar to that of other relaxation processes, the number of inverted particles is significantly reduced, so that the gain coefficient also decreases, and the gain reaches saturation. When I_2 was 1.5 A, the disturbance of the ASE was very small. As I_2 was increased, the ASE exhibited more disturbance, accompanied by Fabry–Pérot resonance. This was related to the low reflectivity of facet and the existence of certain reflectivity of the test system. Improvement measures, including the angled facet structure and development of a wide spectrum of ultra-low reflectivity antireflection coatings, were adopted to minimize this.

The seed laser used in the experiment was continuously tunable for wavelength and power. The amplified output spectrum of the SOA at different bias currents is shown in Fig. 9. The proposed device has excellent gain in the wavelength range of 1510–1590 nm. When I_2 is 1.5 A, 2.0 A, and 2.5 A, it exhibits a side mode suppression ratio (SMSR) greater than 50 dB in the wavelength range
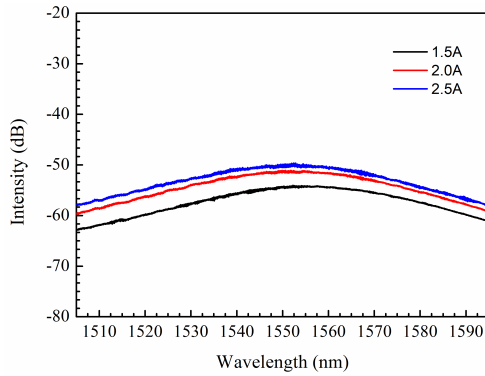
FIGURE 8. Amplified spontaneous emission (ASE) spectrum of the SOA when current $I_1 = 0.3$ A and current $I_2 = 1.5$ A, 2.0 A, and 2.5 A are applied to the ridge waveguide and the tapered waveguide, respectively.

of 1540–1560 nm. The spectrum shows a background signal due to ASE, and while the ASE signal is reduced once the amplifier is pumped with seed laser, no further reduction is seen for greater input powers. This is attributed to the saturation of the SOA. Improved suppression of the ASE background level may be achieved by optimizing the amplifier operation conditions, for instance by adjusting the temperature [24], [25].

As shown in Fig. 10, the saturation output power and gain of the device at 1550 nm were tested in detail. As the input power increased, the output power initially increased linearly, but when the increasing speed slowed down, it tended to saturation. When the input power was increased to 4 mW, the output power reached saturation, and the larger the bias current, the higher the saturated output power. The gain vs. input power curve displays the opposite trend, that is, that the gain decreases exponentially as the input increases. When the input power is 1 mW, the output power is 419 mW and the gain is up to 26.23 dB. As the input power increases, and the device reaches saturated state, the output power increases to 600 mW and the gain reduces to 13.8 dB with an input power of 25 mW. This is because at high input powers a significant number of carriers participate in the stimulated radiation recombination and cannot be quickly replenished. The gain and the output power are limited by the saturation effect, which also helps to reduce the number of longitudinal modes and improve beam quality.

Fig. 10 displays the gain spectrum measuring curve under different bias currents. Fig. 11(a) shows the gain spectrum when the input power is 1 mW. The device works in an unsaturated state, and the 3 dB gain bandwidth is 60 nm when the bias current I_2 is 1.5 A, 2 A and 2.5 A, respectively. The maximum gain $G_{max} = 26.23$ dB is measured at a wavelength of 1550 nm when the bias current is 2.5 A. Fig. 11(b) shows the gain spectrum when the input power is 4 mW. Here, it works in a saturated state, and the 3 dB gain bandwidth is 70 nm when the bias current is 1.5 A, 2 A, and 2.5 A. It is observed that when the input optical signal is unchanged, the gain of the device increases alongside the increase in the injected current. The gain spectrum tends to be flat between
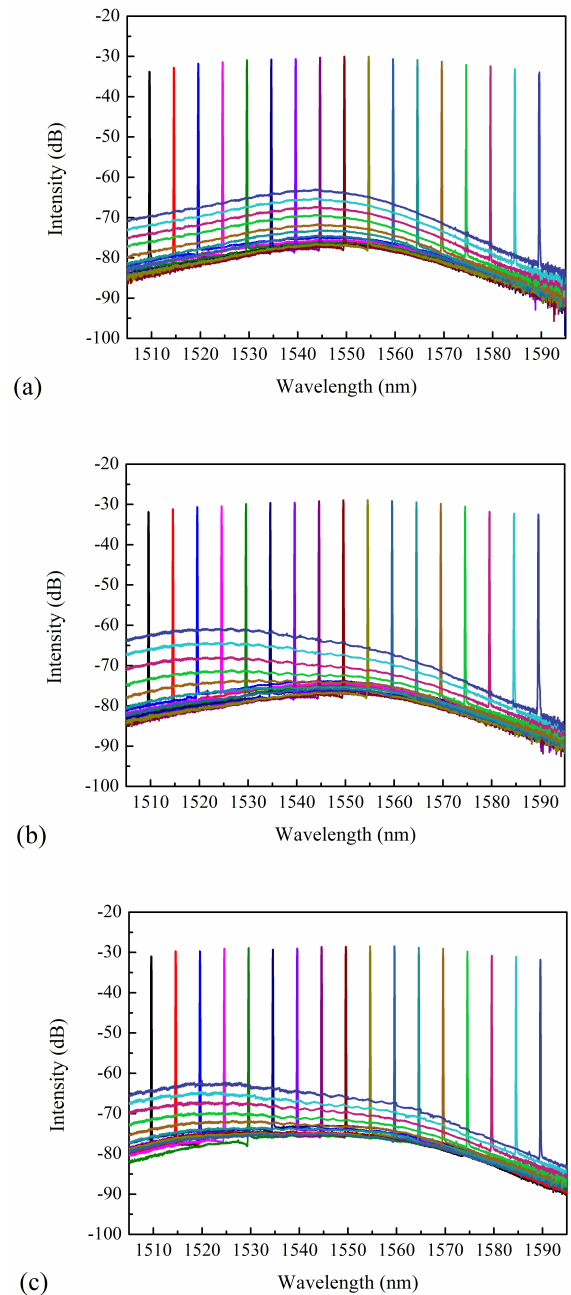

(a)

(b)

(c)

FIGURE 9. Wavelength tuning spectrum. (a) $I_2 = 1.5$ A. (b) $I_2 = 2.0$ A. (c) $I_2 = 2.5$ A.

1540 nm and 1560 nm. As the temperature increases, the gain shows a downward trend as shown in Fig. 11(c).

The linewidth expansion of an SOA is a very important index for practical applications. The narrower the linewidth, the greater the advantage of stimulus emission over spontaneous emission, which means that the number of coherent photons in the cavity increases and the output power increases accordingly. When a narrow linewidth seed laser is input into the SOA, the linewidth of the amplified optical signal changes will directly affect the ability of the system to work properly. Fig. 12 shows the Lorentzian linewidth measurement of the
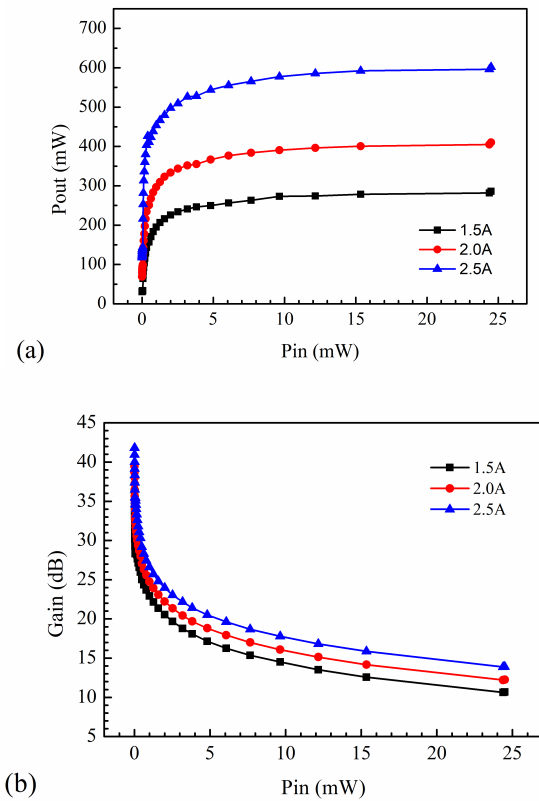
(a)

(b)

FIGURE 10. Seed laser input at 1550 nm wavelength. (a) Measured output power dependence on input power at different bias levels. (b) Measured gain dependence on input power at different bias levels.

seed laser and after the SOA amplification. The linewidth of the seed laser is 94.49 kHz, and the linewidth after SOA amplification is 108.91 kHz. This means that the linewidth after SOA amplification is 1.15 times that of the seed laser. The linewidth measurement system used in the research is calculated based on the integration of the phase noise spectral density function (calculated in Hz^2/Hz). The blue points in Fig. 12 represent the intersection of the frequency noise spectral density function integral curve and the β separation line at different frequencies. The intersection on the far right is the minimum Lorentzian linewidth. Several peaks in the mid-frequency region represent the background noise of the seed laser, and the peaks in the high-frequency region are the background noise of the linewidth measurement system.

In this paper, the beam quality is calculated by measuring the beam divergence angle and using it in the following formula:

$$M^2 = \frac{\pi l \theta}{4\lambda} \tag{10}$$

where the seed laser inputs light of $\lambda = 1550$ nm, which passes through the SOA, and is received and analyzed by a sensor at a distance of $l = 1$ m. The slow axis divergence angle is $\theta_x = 2.495$ mrad, and the fast axis divergence angle $\theta_y = 2.821$ mrad. Equation (10) shows that the slow axis beam quality is 1.263 and the fast axis beam quality is 1.429.
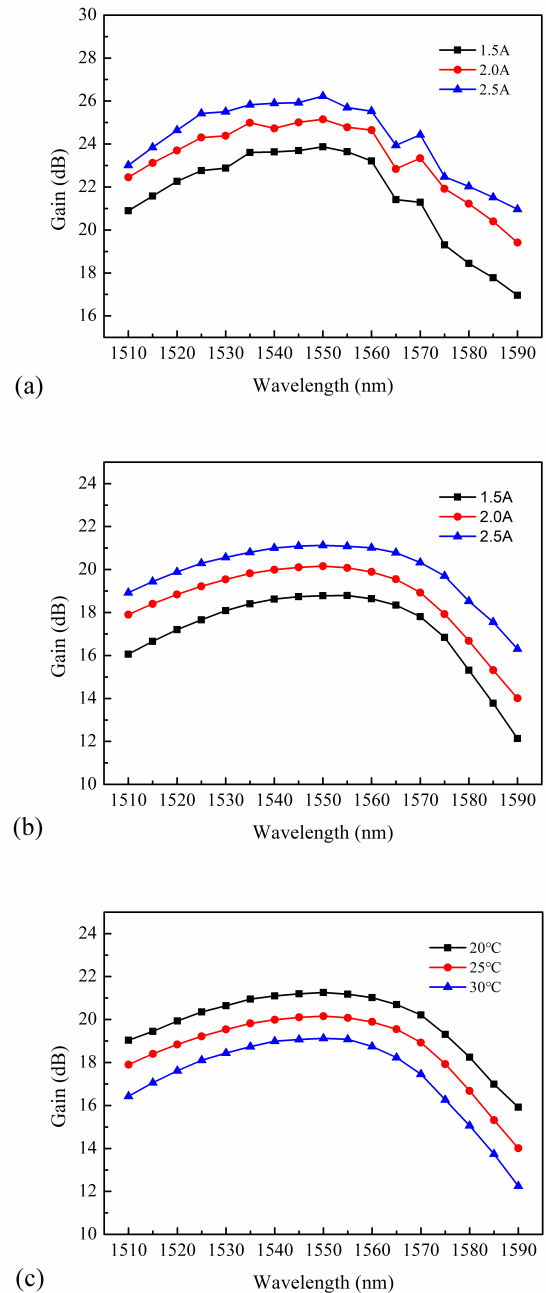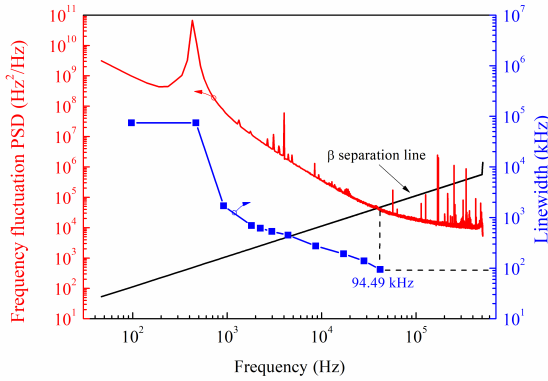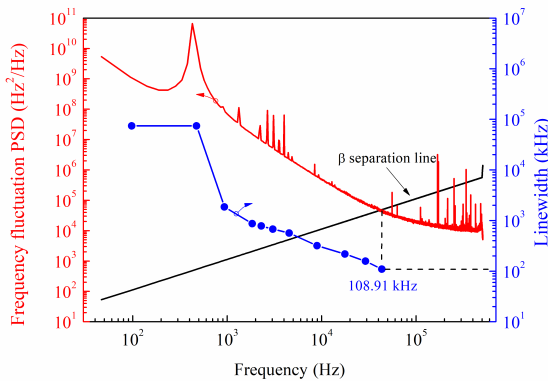
(a)

(b)

(c)

FIGURE 11. Gain spectrum for seed laser with a wavelength range of 1510–1590 nm and current $I_2 = 1.5$ A, 2.0 A, and 2,5 A in the tapered waveguide. (a) Input power of seed laser $P_{in} = 1$ mW. (b) Input power of seed laser $P_{in} = 4$ mW. (c) Measured gain dependence on temperature at $I_2 = 2.0$ A and $P_{in} = 4$ mW.

The excellent beam quality reduces the difficulty of coupling and shaping. Two lenses that compress the fast axis and the slow axis of the spot can be added to the output facet of the SOA to achieve effective coupling of light.

The noise figure is also one of the most important parameters of the SOA, and it is generally measured either by the electrical measurement method or the optical measurement method. In this study, the optical measurement method was adopted, and the measurement block diagram is shown

(a)

(b)

FIGURE 12. Input 1550 nm seed source laser linewidth test result. (a) Linewidth of the seed source laser. (b) Linewidth of the seed source laser after SOA amplification.

FIGURE 13. Noise figure test system.

TABLE 1. Measurement results of the noise figure at different attenuation multiples and comparison with those of other reported SOAs.

P_{out}(mW)	K	P_f(mW)	γ	ρ(dBm/nm)	NF (dB)
600	600	0.1	6000	-53	7.96
600	600	0.2	3000	-52.5	7.95
600	600	0.3	2000	-48.4	7.79

FIGURE 14. The noise figure varies with the bias current I_2 at different temperatures.

in Fig. 13. A laser with a very low spontaneous emission noise spectrum density was injected into the SOA under test by a polarizer and an optical isolator. The SOA output light was attenuated to a safe power level by another optical isolator and a variable optical attenuator (VOA), and then was measured by an OSA and an optical power meter (OPM).

$$NF = 10 \log_{10}(2\gamma\rho/(Kh\nu) + 1/K) \qquad (11)$$

Equation (11) is the expression of the noise figure. The SOA in this paper is polarization-dependent, and the polarization correction factor is about 2. γ is the attenuation multiple of the optical power input to the OSA, given by $\gamma = P_{sat}/P_f$, where P_{sat} is the saturated output power and P_f is the optical power coupled into the OSA. K is the optical gain, expressed by $K = P_{sat}/P_{in}$, where P_{in} is the input power of the SOA. It should be noted that if the spontaneous emission spectrum density of the seed laser is large enough to not be negligible, it is necessary to subtract this spectrum density from the measured total amplified spontaneous emission density to ensure the accuracy of the test results. Table 1 shows the measurement results of the noise figure at different attenuation multiples. The device has a low noise figure of less than 8 dB. As the bias current I_2 increases, the noise figure increases, and as the temperature increases, the noise figure decreases as shown in Fig. 14.
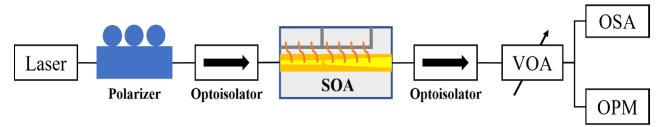
IV. DISCUSSION

The performance characteristics of the SOA fabricated in this study were compared with those of other reported SOAs. The results are listed in Table 1. The SOAs in the literature [26]–[30] are devices based on the master oscillator power amplifier (MOPA) structure. They cannot achieve high saturation power and high gain at the same time. The device prepared in this paper has better performance. The saturated output power reaches 419 mW at 300 mA and bias current of 2.5 A (I_{TAP}), and the maximum small signal gain achieved is 26.23 dB. As the input power continues to increase, the saturated output power reaches 600 mW at 300 mA and bias current of 2.5 A(I_{TAP}), and the gain achieved is 13.8 dB. The Lorentzian linewidth after the SOA is only 1.15 times wider than that of the seed laser. This is a very small linewidth expansion value. These characteristics can be attributed to the large optical cavity structure used in the epitaxial structure. By appropriately reducing the active area confinement factor and increasing the thickness of the N waveguide, the optical field distribution is broadened, increasing the saturated output power. In addition, using a large-angle tapered amplification structure allows the device to maintain single-mode operation through self-focusing of the beam under high current injection, and its slow axis and fast axis beam quality are 1.263 and 1.429, respectively.

TABLE 2. Comparison of parameters between devices reported in previous studies and the proposed SOA.

References	L_{RW} (mm)	L_{TAP} (mm)	α(°)	I_1/I_2 (mA)	P_{out} (mW)	G(dB)
Ref. [30]	1	1.5	4	300/4000	> 400	~16.4
Ref. [29]	1.155	1.2	10	300/800	210	~9.6
Ref. [26]	1	2.5	4	500/3500	300	~25.6
Ref. [27]	1	2	4	200/3000	380	~22.8
Ref. [28]	1	2	4	300/3000	375	~15.7
This paper	1	1.5	10.4	300/2500	419	26.23

V. CONCLUSION

In this study, we designed and fabricated a broad-spectrum, high-power, high-gain, small linewidth expansion two-stage amplified SOA based on the epitaxial structure, and investigated the performance of the SOA for various bias currents in the tapered waveguide section at 25 °C. The results show that the SOA has a 3 dB gain bandwidth of 70 nm. When the input wavelength is 1550 nm, the saturated output power can reach up to 600 mW, and the corresponding gain is 13.8 dB. When the saturated output power is 419 mW, the gain can be as high as 26.23 dB. The Lorentzian linewidth after the SOA is only 1.15 times wider than that of the seed laser. Future work will continue to optimize the performance of this SOA and apply this device to high-power, high gain, broad-spectrum, and narrow linewidth equipment such as all-solid-state lidar and space laser communications.

REFERENCES

[1] M. Xia and H. Ghafouri-Shiraz, "Wavelength-dependent femtosecond pulse amplification in wideband tapered-waveguide quantum well semiconductor optical amplifiers," *Appl. Opt.*, vol. 54, no. 35, pp. 10524–10531, Dec. 2015, doi: 10.1364/AO.54.010524.

[2] J. S. Osinski, D. Mehuys, D. F. Welch, R. G. Waarts, J. S. Major, K. M. Dzurko, and R. J. Lang, "Phased array of high-power, coherent, monolithic flared amplifier master oscillator power amplifiers," *Appl. Phys. Lett.*, vol. 66, no. 5, pp. 556–558, Jan. 1995, doi: 10.1063/1.114011.

[3] P. Albrodt, M. T. Jamal, A. K. Hansen, O. B. Jensen, M. Niemeyer, G. Blume, K. Paschke, P. Crump, J. Hamperl, P. Georges, and G. Lucas-Leclin, "Recent progress in brightness scaling by coherent beam combining of tapered amplifiers for efficient high power frequency doubling," *Proc. SPIE*, vol. 10900, Mar. 2019, Art. no. 109000O.

[4] S. Strohmaier, C. Tillkorn, P. Olschowsky, and J. Hostetler, "High-power, high-brightness direct-diode lasers," *Opt. Photon. News*, vol. 21, no. 10, pp. 24–29, Oct. 2010, doi: 10.1364/OPN.21.10.000024.

[5] K. J. Creedon, S. M. Redmond, G. M. Smith, L. J. Missaggia, M. K. Connors, J. E. Kansky, T. Y. Fan, G. W. Turner, and A. Sanchez-Rubio, "High efficiency coherent beam combining of semiconductor optical amplifiers," *Opt. Lett.*, vol. 37, no. 23, pp. 5006–5008, Dec. 2012, doi: 10.1364/OL.37.005006.

[6] P. Albrodt, M. T. Jamal, A. K. Hansen, O. B. Jensen, G. Blume, K. Paschke, P. Crump, P. Georges, and G. Lucas-Leclin, "Coherent combining of high brightness tapered amplifiers for efficient non-linear conversion," *Opt. Exp.*, vol. 27, no. 2, pp. 928–937, Jan. 2019, doi: 10.1364/OE.27.000928.

[7] W. Loh, J. J. Plant, J. Klamkin, J. P. Donnelly, F. J. O'Donnell, R. J. Ram, and P. W. Juodawlkis, "Noise figure of watt-class ultralow-confinement semiconductor optical amplifiers," *IEEE J. Quantum Electron.*, vol. 47, no. 1, pp. 66–75, Jan. 2011, doi: 10.1109/JQE.2010.2085422.

[8] P. W. Juodawlkis, J. J. Plant, W. Loh, L. J. Missaggia, F. J. O'Donnell, D. C. Oakley, A. Napoleone, J. Klamkin, J. T. Gopinath, D. J. Ripin, S. Gee, P. J. Delfyett, and J. P. Donnelly, "High-power, low-noise 1.5-µm slab-coupled optical waveguide (SCOW) emitters: Physics, devices, and applications," *IEEE J. Sel. Topics Quantum Electron.*, vol. 17, no. 6, pp. 1698–1714, Dec. 2011, doi: 10.1109/JSTQE.2011.2126041.

[9] M. A. Ummy, S. Bikorimana, and R. Dorsinville, "A novel technique for designing high power semiconductor optical amplifier (SOA)-based tunable fiber compound-ring lasers using low power optical components," *Appl. Sci.*, vol. 7, no. 5, p. 478, May 2017, doi: 10.3390/app7050478.

[10] X. U. Hang et al., "EDFA-induced additional beat noise in long distance distributed optical fiber sensing system," *J. Fudan Univ., Natural Sci.*, vol. 58, no. 4, pp. 454–459, Aug. 2019, doi: 10.15943/j.cnki.fdxb-jns.2019.04.006.

[11] L. Yi, Z. Meng, Z. Hu, and Y. Hu, "Design of a low-noise Er-doped-fiber-amplifier (EDFA) for fiber hydrophone system," *Proc. SPIE*, vol. 6830, Jan. 2008, Art. no. 68302B.

[12] M. C. Wu, N. A. Olsson, D. Sivco, and A. Y. Cho, "A 970 nm strained-layer InGaAs/GaAlAs quantum well laser for pumping an erbium-doped optical fiber amplifier," *Appl. Phys. Lett.*, vol. 56, no. 3, pp. 221–223, Jan. 1990, doi: 10.1063/1.102837.

[13] T. Shindo, W. Kobayashi, N. Fujiwara, Y. Ohiso, K. Hasebe, H. Ishii, and M. Itoh, "High modulated output power over 9.0 dBm with 1570-nm wavelength SOA assisted extended reach EADFB laser (AXEL)," *IEEE J. Sel. Topics Quantum Electron.*, vol. 23, no. 6, Nov./Dec. 2017, Art. no. 1500607, doi: 10.1109/JSTQE.2017.2687042.

[14] R. C. Figueiredo, T. Sutili, N. S. Ribeiro, C. M. Gallep, and E. Conforti, "Semiconductor optical amplifier space switch with symmetrical thin-film resistive current injection," *J. Lightw. Technol.*, vol. 35, no. 2, pp. 280–287, Jan. 15, 2017, doi: 10.1109/JLT.2016.2635202.

[15] S. P. Ó. Dúill, P. Landais, and L. P. Barry, "Estimation of the performance improvement of pre-amplified PAM4 systems when using multi-section semiconductor optical amplifiers," *Appl. Sci.*, vol. 7, no. 9, p. 908, Sep. 2017, doi: 10.3390/app7090908.

[16] Z. Zhu, X. Li, and Y. Xi, "A polarization insensitive semiconductor optical amplifier," *IEEE Photon. Technol. Lett.*, vol. 28, no. 17, pp. 1831–1834, Sep. 1, 2016, doi: 10.1109/LPT.2016.2573291.

[17] S. Mazzucato, H. Carrère, X. Marie, T. Amand, M. Achouche, C. Caillaud, and R. Brenot, "Gain, amplified spontaneous emission and noise figure of bulk InGaAs/InGaAsP/InP semiconductor optical amplifiers," *IET Optoelectron.*, vol. 9, no. 2, pp. 52–60, Apr. 2015, doi: 10.1049/iet-opt.2014.0064.

[18] S. Koenig, R. Bonk, H. Schmuck, W. Poehlmann, T. Pfeiffer, C. Koos, W. Freude, and J. Leuthold, "Amplification of advanced modulation formats with a semiconductor optical amplifier cascade," *Opt. Exp.*, vol. 22, no. 15, pp. 17854–17871, Jul. 2014, doi: 10.1364/OE.22.017854.

[19] J. E. Nkanta, R. Maldonado-Basilio, K. Khan, A. Benhsaien, S. Abdul-Majid, J. Zhang, and T. J. Hall, "Low polarization-sensitive asymmetric multi-quantum well semiconductor amplifier for next-generation optical access networks," *Opt. Lett.*, vol. 38, no. 16, pp. 3165–3168, Aug. 2013, doi: 10.1364/OL.38.003165.

[20] K. Carney, R. Lennox, R. Maldonado-Basilio, S. Philippe, F. Surre, L. Bradley, and P. Landais, "Method to improve the noise figure and saturation power in multi-contact semiconductor optical amplifiers: Simulation and experiment," *Opt. Exp.*, vol. 21, no. 6, pp. 7180–7195, Mar. 2013, doi: 10.1364/OE.21.007180.

[21] W. Ma, S. Tan, K. Wang, W. Guo, Y. Liu, L. Liao, L. Zhou, J. Zhou, X. Li, L. Liang, and W. Li, "Practical two-dimensional beam steering system using an integrated tunable laser and an optical phased array," *Appl. Opt.*, vol. 59, no. 32, p. 9985, Nov. 2020, doi: 10.1364/AO.403314.

[22] X. Wang, G. Erbert, H. Wenzel, B. Eppich, P. Crump, A. Ginolas, J. Fricke, F. Bugge, M. Spreemann, and G. Tränkle, "High-power, spectrally stabilized, near-diffraction-limited 970 nm laser light source based on truncated-tapered semiconductor optical amplifiers with low confinement factors," *Semicond. Sci. Technol.*, vol. 27, no. 1, p. 10, Dec. 2011, doi: 10.1088/0268-1242/27/1/015010.

[23] S. O'Brien, D. F. Welch, R. A. Parke, D. Mehuys, K. Dzurko, R. J. Lang, R. Waarts, and D. Scifres, "Operating characteristics of a high-power monolithically integrated flared amplifier master oscillator power amplifier," *IEEE J. Quantum Electron.*, vol. 29, no. 6, pp. 2052–2057, Jun. 1993, doi: 10.1109/3.234468.

[24] S. Schwertfeger, J. Wiedmann, B. Sumpf, A. Klehr, F. Dittmar, A. Knauer, G. Erbert, and G. Tränkle, ''7.4 W continuous-wave output power of master oscillator power amplifier system at 1083 nm,'' *Electron. Lett.*, vol. 42, no. 6, pp. 346–347, Mar. 2006, doi: 10.1049/el:20060260.

[25] D. Voigt, E. C. Schilder, R. J. C. Spreeuw, and H. B. van Linden van den Heuvell, ''Characterization of a high-power tapered semiconductor amplifier system,'' *Appl. Phys. B, Lasers Opt.*, vol. 72, no. 3, pp. 279–284, Feb. 2001, doi: 10.1007/s003400100513.

[26] A. Perez-Serrano, J. M. G. Tijero, S. Balle, and I. Esquivias, ''Numerical analysis of the modulation dynamics in an integrated three-section MOPA using a voltage driven traveling-wave model,'' *IEEE J. Sel. Topics Quantum Electron.*, vol. 25, no. 6, Nov./Dec. 2019, Art. no. 3000110, doi: 10.1109/JSTQE.2019.2913037.

[27] C. Pham, F. Van Dijk, E. Vinet, Y. Robert, O. Parillaud, M. Garcia, A. Larrue, M. Faugeron, and A. Rissons, ''Monolithic InP master oscillator power amplifier for free space optical transmissions at 1.5 μm,'' *Proc. SPIE*, vol. 10524, Feb. 2018, Art. no. 105240W.

[28] J. A. Beil, L. Shimomoto, R. B. Swertfeger, S. M. Misak, J. Campbell, J. Thomas, D. Renner, M. Mashanovitch, P. O. Leisher, and R. W. Liptak, ''Improvements to tapered semiconductor MOPA laser design and testing,'' *Proc. SPIE*, vol. 10514, Feb. 2018, Art. no. 105140U.

[29] L. P. Hou, M. Haji, J. Akbar, and J. H. Marsh, ''Narrow linewidth laterally coupled 1.55 μm AlGaInAs/InP distributed feedback lasers integrated with a curved tapered semiconductor optical amplifier,'' *Opt. Lett.*, vol. 37, no. 21, pp. 4525–4527, Oct. 2012, doi: 10.1364/OL.37.004525.

[30] R. B. Swertfeger, J. A. Beil, S. M. Misak, J. Thomas, J. Campbell, D. Renner, M. Mashanovitch, and P. O. Leisher, ''Direct observation of the 2D gain profile in high power tapered semiconductor optical amplifiers,'' in *Proc. 5th Int. Conf. Photon., Opt. Laser Technol.*, San Francisco, CA, USA, 2017, pp. 114–121.

XIN LI was born in Jilin, China. He received the B.S. degree in physics from Jilin Normal University, Siping, China, in 2017, and the M.S. degree in condensed matter physics from the Changchun Institute of Optics, Fine Mechanics and Physics, Chinese Academy of Sciences, Changchun, China, in 2019, where he is currently pursuing the Ph.D. degree in condensed matter physics. His research interests include high-power semiconductor optical amplifiers and high-power narrow-linewidth semiconductor lasers.

LEI LIANG received the B.Sc., M.Sc., and Ph.D. degrees from the College of Electronic Science and Engineering, Jilin University, Changchun, China, in 2009, 2011, and 2014, respectively.

From 2014 to 2020, he was a Research Assistant with the State Key Laboratory of Luminescence and Applications, Changchun Institute of Optics, Fine Mechanics and Physics, Chinese Academy of Sciences, Changchun, where he is currently an Assistant Professor. His research interests include optical waveguide devices, semiconductor lasers, semiconductor optical amplifier, and solid state lidar.

LI JUN WANG was born in Jilin, China, in 1946. He received the B.S. degree in semiconductor devices and the M.S. degree in semiconductor physics and device physics from Jilin University, Changchun, China, in 1973 and 1982, respectively.

From 1986 to 1999, he worked with the Changchun Institute of Physics, Chinese Academy of Sciences. He has been working with the Changchun Institute of Optics, Mechanics, and Physics (CIOMP), Chinese Academy of Sciences, since 1999. He was elected as an Academician of the Chinese Academy of Sciences, in 2013. He has long been engaged in basic and applied research in laser technology and other fields. He led his research team to break through the old framework of the predecessors and theoretically clarify the feasibility of the operation of a watt-level high-power vertical cavity surface emitting laser. New structures and design concepts, such as multi-gain regions were proposed, and a series of key technologies, such as chip manufacturing and device packaging were overcome. He has published 264 SCI and EI papers. He has 39 authorized invention patents and coauthored four monographs. He received the Second Prize of the China's Technology Invention and the Second Prize of the Scientific and Technological Progress.

LI QIN received the B.S. and M.S. degrees in semiconductor devices from Jilin University, Changchun, China, in 1993 and 1996, respectively, and the Ph.D. degree in microelectronics and solid electronics from Jilin University, in 1999. From 2000 to 2002, she held a postdoctoral position at the Changchun Institute of Optics, Mechanics, and Physics (CIOMP), Chinese Academy of Sciences. She has been working with the CIOMP, since 2002. Her research interests include the development of semiconductor laser structure design and chip process optimization. She received the Second Prize of the China's Technological Invention and the Second Prize of the Scientific and Technological Progress.

YONG YI CHEN received the B.S. degree from Nanjing University, Nanjing, China, in 2008, and the Ph.D. degree from the Changchun Institute of Optics, Fine Mechanics and Physics (CIOMP), Chinese Academy of Sciences, Changchun, China, in 2013.

From 2013 to 2016, he was a Research Assistant with CIOMP, where he has been an Assistant Professor, since 2016. He is the coauthor of one book, more than 50 articles, and more than 20 inventions. His research interests include simulation and fabrication of semiconductor lasers and applications, nano scale gratings and photonic crystals, and semiconductor materials. He received the First Prize of Science and Technology of Jilin Province, in 2015.

YU BING WANG received the B.S. degree in electronic science and technology from Jilin University, Jilin, China, in 2012, and the Ph.D. degree in microelectronics and solid-state electronics from the Institute of Semiconductors, Chinese Academy of Sciences, Beijing, China, in 2017.

Since 2017, he has been a Research Assistant with the State Key Laboratory of Luminescence and Applications, Changchun Institute of Optics, Fine Mechanics and Physics, Chinese Academy of Sciences, Jilin. His research interests include high-power semiconductor laser devices and the development of solid-state lidar.

YUE SONG was born in Songyuan, Jilin, China, in 1989. She received the M.S. degree in materials science and engineering from the Changchun University of Science and Technology, in 2015, and the Ph.D. degree in condensed matter physics from the Changchun Institute of Optics, Fine Mechanics and Physics, Chinese Academy of Science, in 2019.

From 2019 to 2021, she was a Research Assistant with the State Key Laboratory of Luminescence and Application, Changchun Institute of Optics, Fine Mechanics and Physics, Chinese Academy of Science. She is the author of more than ten articles. She has submitted an application for an invention patent. Her research interests include high-power semiconductor diode lasers and the reliability and degradation mechanism of diode lasers. She presides the Youth Fund Project of National Natural Science Foundation of China and joins six science research programs and science research works.

YU XIN LEI received the Ph.D. degree in condensed state physics from the Changchun Institute of Optics, Fine Mechanics and Physics, University of Chinese Academy of Sciences, China, in 2019. Since 2019, she has been a Research Assistant with the State Key Laboratory of Luminescence and Applications, Changchun Institute of Optics, Fine Mechanics and Physics, Chinese Academy of Sciences. Her research interests include high-power high-beam quality semiconductor lasers and high-power narrow-linewidth semiconductor lasers.

PENG JIA was born in 1986. He received the Ph.D. degree in condensed matter physics from the University of Chinese Academy of Sciences, Changchun, China, in 2015. He is currently a Research Assistant Professor with the Changchun Institute of Optics, Fine Mechanic and Physics. His research interests include single mode DBR laser diode and high-beam quality laser diode.

YU GANG ZENG was born in Luzhou, Sichuan, China, in 1978. He received the B.S. degree in material sciences and engineering from Tsinghua University, China, in 2002, and the Ph.D. degree in microelectronics and solid-state electronics from the Institute of Semiconductors, Chinese Academy of Sciences, China, in 2008.

From 2008 to 2010, he was a Research Assistant with the Changchun Institute of Optics, Fine Mechanics and Physics (CIOMP), Chinese Academy of Sciences, where he has been an Associate Researcher, since 2010. He is the author of more than 30 articles. His research interests include the development of III-V alloys of high-power semiconductor lasers and the epitaxy technologies, such as MOCVD and MBE.

CHUAN TAO ZHENG received the M.S. and Ph.D. degrees from the College of Electronic Science and Engineering, Jilin University, China, in 2007 and 2010, respectively.

He is currently a Full Professor with Jilin University. His research interests include optoelectronic devices and their applications in gas sensing. He has published more than 170 scientific journal articles in the above technical fields as a first author or corresponding author.

HUAN ZHAO received the B.S. degree from the College of Electronic Science and Engineering, Jilin University, China, in 2017. He is currently pursuing the Ph.D. degree in circuit and system. His research interests include hybrid integrated laser and optical waveguide device.

• • •